Title: Bomb radiocarbon evidence for strong global carbon uptake and turnover in terrestrial vegetation

Authors: Heather D. Graven[1,*], Hamish Warren[1], Holly K. Gibbs[2], Samar Khatiwala[3], Charles Koven[4], Joanna Lester[1], Ingeborg Levin[5,†], Seth A. Spawn-Lee[6,7], and Will Wieder[8]

Affiliations:

[1]Department of Physics, Imperial College London, UK

[2]Nelson Institute for Environmental Studies and the Department of Geography, University of Wisconsin-Madison, USA

[3]Department of Earth Sciences, University of Oxford, UK

[4]Climate and Ecosystem Sciences Division, Lawrence Berkeley National Laboratory, USA

[5]Institute of Environmental Physics, Heidelberg University, Germany

[6]Department of Integrative Biology, University of Wisconsin-Madison, USA

[7]The Nature Conservancy, USA

[8]Climate & Global Dynamics, National Center for Atmospheric Research, and Institute of Arctic and Alpine Research, University of Colorado, USA

[*]Corresponding author. Email: h.graven@imperial.ac.uk

[†]Deceased

Abstract: Vegetation and soils are taking up approximately 30% of anthropogenic CO_2 emissions because of small imbalances in large gross carbon exchanges from productivity and turnover that are poorly constrained. We combine a new budget of radiocarbon (^{14}C) produced by nuclear bomb testing in the 1960s with model simulations to evaluate carbon cycling in terrestrial vegetation. We find that most state-of-the-art vegetation models used in the Coupled Model Intercomparison Project underestimate the ^{14}C accumulation in vegetation biomass. Our findings, combined with constraints on vegetation carbon stocks and productivity trends, imply that net primary productivity is likely at least 80 PgC/yr presently, compared to 43-76 PgC/yr predicted by current models. Storage of anthropogenic carbon in terrestrial vegetation is likely more short-lived and vulnerable than previously predicted.

One-Sentence Summary: Carbon uptake into vegetation is underestimated, but the carbon is turned over quickly.

Main Text:

The processes contributing to the net sink of CO_2 in the terrestrial biosphere are not yet well understood and will likely change in the future (*1*), making it difficult to predict future climate change and create effective mitigation and adaptation policies. Future climate predictions require robust representation of the global carbon cycle, which is challenging when basic properties still have large uncertainties. In particular, observational constraints on global net primary productivity (NPP) - the rate of creation of new plant tissues and products - and on carbon

turnover rates are lacking. Estimates of global NPP rely on statistical or model-based estimates that use site-scale data (*2*); however, it is very difficult to measure all components of NPP (*3*) and there are not many sites with comprehensive measurements, especially in the tropics (*4*). A large range of global NPP of 43-76 PgC/yr is currently simulated by models (*5, 6*), and models do not generally show a strong trend over the 20th century, in conflict with the trend found for gross primary productivity (+30%) (*7*), which is typically twice as large as NPP. Here we provide global-scale constraints on NPP and carbon turnover by analyzing radiocarbon (^{14}C) produced by nuclear bomb testing and models of the terrestrial biosphere and vegetation.

Global bomb radiocarbon budget

Nuclear bomb testing in the 1950s and 1960s produced excess radiocarbon (^{14}C) in the atmosphere (Figure 1a), which was assimilated into the terrestrial biosphere and ocean through photosynthesis and air-sea gas exchange over time. Tracking how ^{14}C accumulated in the terrestrial biosphere after the bomb testing can therefore enable evaluation of the rates of carbon uptake and turnover (*8*). However, the global accumulation of ^{14}C in the biosphere cannot be observed directly: from new leaves to highly aged soil carbon, there is too much heterogeneity in ^{14}C content in the biosphere.

We use a budgeting approach to diagnose the ^{14}C accumulation in the terrestrial biosphere caused by bomb testing in order to evaluate carbon cycling in terrestrial biosphere models. In this approach, the ^{14}C accumulation in the terrestrial biosphere is calculated using observations in the stratosphere and troposphere and observationally-constrained ocean models to close the ^{14}C budget. In contrast to prior work (*9*) that examined the period 1945-2000, here we focus on the period 1963-67, when atmospheric ^{14}C was highly elevated relative to the biosphere but when no significant detonations took place (blue area in Figure 1a). Therefore, total ^{14}C in the Earth system was roughly constant but exchanged between reservoirs over 1963-67. This allows us to focus on the period where there is good observational coverage of the stratosphere by aircraft and balloon sampling, and to avoid uncertainty and assumptions with calculating the total ^{14}C produced by the bombs and estimating the pre-bomb ^{14}C content. Another advantage of focusing on 1963-67 is that we sharpen the constraint on ^{14}C uptake and turnover in vegetation, where the ^{14}C first entered the terrestrial biosphere, before much ^{14}C was transferred to litter and soil pools.

We use stratospheric data originally published in reports of the Health and Safety Laboratories, which were reassessed and recalculated with corrected standard values (*10-12*) and used in an atmospheric model to calculate global stratospheric ^{14}C inventories (*11*) (Figure 1). Tropospheric ^{14}C inventories were calculated from global compilations recently produced for modelling purposes (*13, 14*). Ocean ^{14}C simulations (*15-18*) that match revised ocean ^{14}C inventories (*19, 20*) from the 1970s (GEOSECS) and 1990s (WOCE) were used for ocean ^{14}C inventories.

After the ^{14}C was initially deposited in the stratosphere, the stratosphere lost roughly 200×10^{26} atoms of ^{14}C through mixing of the ^{14}C into the troposphere over 1963-67, which experienced a net gain of about 40×10^{26} atoms. The ocean gained about 80×10^{26} atoms through air-sea exchange (Figure 1b). We estimate that the terrestrial biosphere therefore must have accumulated $86\pm18\times10^{26}$ atoms (95% confidence) (*21*) over 1963-67 (Figure 1c) as the assimilation of ^{14}C outpaced the turnover of ^{14}C back to the air.

Terrestrial biospheric ^{14}C accumulation in the CESM2 model

The terrestrial biospheric ^{14}C accumulation over 1963-67 provides a new constraint on coupled climate-carbon cycle models (also known as Earth system models or ESMs), which are used to inform global climate policy but have particularly uncertain terrestrial carbon cycle components due to the heterogeneity and complexity of land ecosystems. Simulations of the only such land model to simulate ^{14}C explicitly within an ESM, the Community Land Model version 5.0 (CLM5.0) (*22*), accumulate a much lower amount of ^{14}C in the terrestrial biosphere (about 40×10^{26} atoms) than our observation-based estimate ($86\pm18\times10^{26}$ atoms, Figure 1c). Simulations of CLM5.0 driven with observed climate data (CLM5.0-unc, "uncoupled") (*23*) and coupled model simulations of the Community Earth System Model 2 (*24*) Large Ensemble Project (CESM2-LENS) (*25*)(*26*) following the Coupled Model Intercomparison Project (CMIP) phase 6 historical (concentration-driven) simulation protocol show similar ^{14}C accumulation, and the spread across 9 ensemble members is small (Figure 1c). CLM5.0-unc results are similar to another offline simulation of CLM5.0 that suggested the ^{14}C accumulated in the terrestrial biosphere in the 1960s could be too small (*27*).

In 1963-67 not much bomb ^{14}C had yet entered the soil; most biospheric bomb ^{14}C was in vegetation (Figure 1c). In CESM2-LENS, 56% of the ^{14}C accumulated in vegetation, with only 18% in litter and coarse woody debris and 26% in soils over 1963-67. If the ^{14}C accumulation in vegetation in CESM2 were correct, then the ^{14}C accumulation in non-vegetation pools would have to be >3 times larger than simulated in CESM2-LENS and >75% of the total ^{14}C accumulation to match the observation-based estimate. It is unlikely that more than half of the biospheric ^{14}C accumulation over 1963-67 occurred in dead plant material and soils since the peak in global mean tropospheric ^{14}C occurred only in 1964-65.

We thus conclude that the ^{14}C accumulation in vegetation over 1963-67 in CESM2 is too low (Figure 1). The underestimate for vegetation could be because the NPP in the model is too low, so that not enough ^{14}C enters the vegetation, and/or because carbon is misallocated between short-lived vs long-lived pools, so that ^{14}C is turned over too quickly.

Vegetation model emulators and model-data comparisons

CESM2 is the only Earth system model with explicit simulations of ^{14}C available. Therefore, to simulate the ^{14}C accumulation in other models as well as to explore the sensitivity of the ^{14}C accumulation to NPP and carbon stocks, we need to construct emulator models. We found that the variables included in CMIP were not sufficient to construct a reliable emulator model for the whole terrestrial biosphere for CESM2, but that ^{14}C in vegetation could be modeled reliably (Figures 2-4).

We focus now on analyzing the ^{14}C accumulation only in vegetation in models over 1963-67. We constructed a simple emulator model for woody (long-lived: stem and coarse roots) and non-woody vegetation biomass (short-lived: leaves, fine roots and other pools), run on each model grid cell (*21*). We applied the emulator model to CESM2-LENS member 1001.001 and to models from CMIP5 and CMIP6 that reported the necessary variables. We examine global sums for woody and non-woody pools across all biomes and grid cells (Figures 2-4 and S1), so that global non-woody vegetation biomass includes the non-woody vegetation biomass in forests as well as other biomes. We compare with satellite-based vegetation carbon products (*29-31*) that

omit leaf carbon in forests, so we estimated global total leaf carbon in forests to be 14.3 PgC (based on Table S5 in reference (*32*)) and added this to the observation-based estimates of vegetation carbon stocks.

To evaluate the vegetation ^{14}C simulations, we estimate the true ^{14}C accumulation in vegetation by subtracting the ^{14}C accumulation in litter, coarse woody debris and soils simulated by CESM2-LENS member 1001.001 from the observation-based total terrestrial biosphere ^{14}C accumulation over 1963-67. We allow the uncertainty in non-vegetation ^{14}C accumulation to be ±100% (95% confidence) (*21*), even though CESM2/CLM5 is in fact likely to overestimate this ^{14}C accumulation since its proportion of fresh carbon in both surface and sub-surface soils has been shown to be too high (*33*). Our estimate of vegetation ^{14}C accumulation is $69 \pm 24 \times 10^{26}$ atoms (95% confidence) over 1963-67 at 95% confidence, which allows for a possible range of 43-100% of biospheric ^{14}C accumulation in vegetation.

Most of the CMIP5 and CMIP6 vegetation emulator models underestimate the observation-based vegetation ^{14}C accumulation over 1963-67 (5 of 7 models, Figure 2). The two models that match the observation-based vegetation ^{14}C accumulation have high NPP of more than 68 PgC/yr in 1965 (Figure 2b, Figure S1, Table S1). One of the two models is from CMIP5 (IPSL5), whereas the CMIP6 version of that model (IPSL6) has much lower NPP and underestimates the observation-based vegetation bomb ^{14}C inventory. The other model matching the observation-based vegetation bomb ^{14}C inventory, CanESM5 from CMIP6, has high NPP and allocates a large fraction of its NPP to wood (68% in 1965), in contrast to other models that allocate 22-43% of NPP to wood (Table S1).

Overall, the ^{14}C accumulation in vegetation over 1963-67 shows a strong relationship with NPP but not with vegetation carbon stock (Figure 2). This indicates that higher NPP increases ^{14}C accumulation in vegetation over 1963-67 but higher carbon stock (and slower turnover rate) generally does not. Two versions of the MRI model lie below a regression line between ^{14}C accumulation in vegetation and NPP for the other five models (Figure 2b). The MRI models allocate the highest fraction of NPP to non-woody vegetation (76-78% to non-woody, 22-24% to woody) and their non-woody annual NPP is similar to their non-woody carbon stock (Table S1), which indicates a very high level of productivity per unit biomass and fast turnover rate. Therefore, the flux of ^{14}C into non-woody vegetation in the MRI models is large but it is turned over quickly and the ^{14}C accumulation in non-woody vegetation is among the lowest (Figure 3a).

There are differing controls on ^{14}C accumulation over 1963-67 in non-woody vs woody vegetation biomass in the emulator models (Figures 3, S2 and S3). Accumulation of ^{14}C in longer-lived woody vegetation is sensitive to NPP, while accumulation of ^{14}C in shorter-lived non-woody vegetation is more sensitive to the carbon stock. At higher stocks of non-woody vegetation carbon, ^{14}C accumulation in non-woody vegetation is also sensitive to NPP. The patterns found for scaling experiments in the CESM2 vegetation emulator (contours in Figure 3) are similar to the patterns found for the other vegetation model emulators (colored symbols in Figure 3).

The patterns in Figure 3 indicate that underestimated ^{14}C accumulation in vegetation over 1963-67 is due to underestimated NPP or underestimated non-woody vegetation biomass in models. Only IPSL6 underestimates the total vegetation carbon stock estimated with satellite data (Figure 2c, Figure S4), so increasing non-woody carbon stock in the models requires that carbon shifts

from woody biomass (stems and coarse roots) to non-woody biomass (leaves, fine roots and other biomass) by adjustment of their turnover rates. The models tend to underestimate belowground vegetation carbon stocks (*29, 30*) (Figure S5), so shifting aboveground woody carbon (stems) to belowground non-woody carbon (fine roots) in particular may be required. On the other hand, NPP in woody (or non-woody) vegetation could be increased in the models without necessarily affecting carbon stocks, if modelled turnover rates are simultaneously increased.

The regression between vegetation ^{14}C accumulation and NPP (R^2>0.99), excluding the MRI models that have very high non-woody NPP, suggests that NPP in 1965 should have been at least 63 PgC/yr (the value of NPP at the intersection of the regression line and ^{14}C accumulation uncertainty range in Figure 2b). However, only 16% of all CMIP6 models have NPP higher than 63 PgC/yr in 1965 (Figure 2d, Table S2). Considering that total carbon assimilation (Gross Primary Productivity or GPP) increased by ~30% over the 20th century (*7*), if carbon uptake efficiency (NPP/GPP) did not change significantly then NPP should be at least 80 PgC/yr presently, while it is only 43-76 PgC/yr in current models (*5*).

Implications for the carbon cycle

The simulations of ^{14}C we analysed provide evidence that CESM2 and most other CMIP6 models underestimate the magnitude of NPP in the 1960s. The minimum NPP of 63 PgC/yr in 1965 and 80 PgC/yr recently (applying a 30% increase following (*7*)) that is implied by our analysis of bomb ^{14}C in vegetation is higher than simulated in most CMIP6 models (*5*) (Figure 2) but within the higher end of the range of observation-based estimates of GPP (*34-37*), assuming roughly 50% NPP/GPP. The global NPP/GPP ratio might increase slightly in the future (*38*), but we are not aware of any evidence for a historical trend. The average NPP in CMIP6 models actually decreased in comparison with CMIP5 models (*5, 39*), which likely degraded the model cohort rather than improved it.

Our results highlight parametric and structural uncertainties in model simulations of leaf-level photosynthesis and stomatal conductance, nutrient limitation, autotrophic respiration, carbon allocation, mortality and turnover. For example, replacing the widely-used assumption of homogeneity in wood carbon turnover rates at a given location (*40*) with vegetation demographic models (*41*) that allow distinct populations of fast-growing versus long-lived trees may improve ^{14}C accumulation, where the former are able to rapidly take up ^{14}C while the latter dominate the overall biomass pool (*42*). However, since ^{14}C accumulation over 1963-67 is higher in woody than non-woody vegetation (Figures 3, S1 and S4), it is likely that increasing NPP to woody vegetation in models that underestimate ^{14}C accumulation is required. Satisfying observational constraints on carbon stocks while increasing NPP will require that the rate of carbon turnover in the models also increases.

A range of 41-64 PgC/yr for NPP was found in a previous study (*9*) using a ^{14}C budget to diagnose the bomb-produced ^{14}C in the biosphere, and then using this budget to fit parameters in a simple 3-box global biosphere model (*43*). Our evaluation of state-of-the-art global biosphere models suggests that the ^{14}C budget in the 1960s cannot be met with NPP lower than 63 PgC/yr in current model formulations (Figure 2b). This is in fact consistent with reference (*9*) whose budget was not closed in the 1960s and instead included a residual “hidden sink”, which must be in the terrestrial biosphere.

Radiocarbon data provide powerful and unique insights on carbon cycling and model evaluation, but they have been underutilized due to the low number of models simulating ^{14}C. In addition to the observation-based global ^{14}C accumulation used here and soil carbon ^{14}C data used previously to evaluate CMIP models (*33*, *44*), other data including ^{14}C in specific soil compounds, in respiration or in atmospheric CO_2 could be used to evaluate more processes in models that simulate ^{14}C. Analyzing the 1963-67 period allowed us to focus on vegetation, but longer analysis of subsequent decades would enable critical insights on whole ecosystem cycling including litter and soil (Figure 1c). Within vegetation alone, ^{14}C simulations strongly diverge over time (Figure 2a) and there are large differences between models in their spatial distribution of ^{14}C accumulation, NPP and carbon stock (Figure 4 and S6). Spatial differences in ^{14}C accumulation between models are at least a factor of two but up to a factor of 10 for non-woody vegetation in northern temperate and boreal regions. Additional ^{14}C data-model comparison will enable more constraints on various processes. Also, since we estimated the 1963-67 ^{14}C accumulation in litter and soils based on the CESM-LENS simulations (with ±100% uncertainty), further analysis of ^{14}C through all biospheric pools would help to refine the constraints on vegetation.

The vegetation emulator model we used represents the ^{14}C explicitly simulated in CESM2 well (Figures 2-4), but the emulator could not be evaluated for other models and emulators for litter and soil pools could not be constructed with the limited variables in the CMIP output. Ensuring an accurate representation of ^{14}C in biospheric models requires that the models explicitly simulate ^{14}C, which only requires one additional tracer to be added in a simple way (*21*). New methods for fast spin up could be exploited (*45-47*). As requested for CMIP6 (*48*), we strongly recommend that modelling groups implement ^{14}C in ESMs and in stand-alone models, and report these results to CMIP and related activities to enable model assessment and scientific understanding.

Accurate simulation of vegetation and total biospheric carbon uptake and turnover is critical to understanding historical and future anthropogenic carbon storage in terrestrial ecosystems, both for natural sinks of CO_2 as well as for ‘nature-based solutions’ that aim to remove atmospheric CO_2 by increasing land ecosystem carbon. Our analysis shows that the uptake of carbon via NPP and the rate of carbon turnover in models must both be increased, which will increase the turnover of anthropogenic carbon in the terrestrial biosphere. Since the uptake and turnover of carbon are the main controls on the anthropogenic CO_2 sink in the terrestrial biosphere, this study shows that the storage of anthropogenic carbon in the terrestrial biosphere is likely more short-lived and more vulnerable to future changes than previously thought.

References and Notes

1. P. Friedlingstein *et al.*, Global Carbon Budget 2023. *Earth Syst. Sci. Data* **15**, 5301-5369 (2023).
2. A. Ito, A historical meta-analysis of global terrestrial net primary productivity: are estimates converging? *Global Change Biology* **17**, 3161-3175 (2011).
3. D. A. Clark *et al.*, Measuring Net Primary Production in Forests: Concepts and Field Methods. *Ecological Applications* **11**, 356-370 (2001).
4. R. J. Olson, J.M.O. Scurlock, S.D. Prince, D.L. Zheng, and K.R. Johnson, O. R. N. L. D. A. A. Center, Ed. (Oak Ridge, Tennessee, USA, 2013).

5. R. M. Varney, S. E. Chadburn, E. J. Burke, P. M. Cox, Evaluation of soil carbon simulation in CMIP6 Earth system models. *Biogeosciences* **19**, 4671-4704 (2022).
6. M. Zhao, F. A. Heinsch, R. R. Nemani, S. W. Running, Improvements of the MODIS terrestrial gross and net primary production global data set. *Remote Sensing of Environment* **95**, 164-176 (2005).
7. J. E. Campbell *et al.*, Large historical growth in global terrestrial gross primary production. *Nature* **544**, 84-87 (2017).
8. S. E. Trumbore, Age of Soil Organic Matter and Soil Respiration: Radiocarbon Constraints on Belowground C Dynamics. *Ecological Applications* **10**, 399-411 (2000).
9. T. Naegler, I. Levin, Observation-based global biospheric excess radiocarbon inventory 1963–2005. *Journal of Geophysical Research* **114**, D17302 (2009).
10. T. Naegler, Simulating bomb radiocarbon: Consequences for the global carbon cycle, PhD Thesis, Univ. of Heidelberg, Heidelberg, Germany (2005).
11. T. Naegler, I. Levin, Closing the global radiocarbon budget 1945–2005. *J Geophys Res* **111**, D12311 (2006).
12. V. Hesshaimer, I. Levin, Revision of the stratospheric bomb $^{14}CO_2$ inventory. *J Geophys Res* **105**, 11641-11658 (2000).
13. H. Graven *et al.*, Compiled records of carbon isotopes in atmospheric CO_2 for historical simulations in CMIP6. *Geosci. Model Dev.* **10**, 4405-4417 (2017).
14. M. Meinshausen *et al.*, Historical greenhouse gas concentrations for climate modelling (CMIP6). *Geosci Model Dev* **10**, 2057-2116 (2017).
15. H. D. Graven, N. Gruber, R. Key, S. Khatiwala, X. Giraud, Changing controls on oceanic radiocarbon: New insights on shallow-to-deep ocean exchange and anthropogenic CO_2 uptake. *J Geophys Res* **117**, C10005 (2012).
16. S. Khatiwala, H. Graven, S. Payne, P. Heimbach, Changes to the Air-Sea Flux and Distribution of Radiocarbon in the Ocean Over the 21st Century. *Geophysical Research Letters* **45**, 5617-5626 (2018).
17. B. Pookkandy, H. Graven, A. Martin, Contemporary oceanic radiocarbon response to ocean circulation changes. *Climate Dynamics*, (2023).
18. J. G. Lester, "Changes in oceanic radiocarbon and CFCs since the 1990s. doi: 10.5281/zenodo.8242144," (Zenodo, 2023).
19. T. Naegler, Reconciliation of excess ^{14}C-constrained global CO_2 piston velocity estimates. *Tellus B* **61**, 372-384 (2009).
20. S. Peacock, Debate over the ocean bomb radiocarbon sink: Closing the gap. *Global Biogeochemical Cycles* **18**, (2004).
21. Materials and methods are available as supplementary materials online.
22. D. M. Lawrence *et al.*, The Community Land Model Version 5: Description of New Features, Benchmarking, and Impact of Forcing Uncertainty. *Journal of Advances in Modeling Earth Systems* **11**, 4245-4287 (2019).
23. CLM5.0 data are archived and publicly available at the UCAR/NCAR Climate Data Gateway (https://doi.org/10.5065/d6154fwh).
24. G. Danabasoglu *et al.*, The Community Earth System Model Version 2 (CESM2). *Journal of Advances in Modeling Earth Systems* **12**, e2019MS001916 (2020).
25. K. B. Rodgers *et al.*, Ubiquity of human-induced changes in climate variability. *Earth Syst. Dynam.* **12**, 1393-1411 (2021).
26. CESM2-LENS data are available at https://www.cesm.ucar.edu/community-projects/lens2

27. T. Frischknecht, A. Ekici, F. Joos, Radiocarbon in the Land and Ocean Components of the Community Earth System Model. *Global Biogeochemical Cycles* **36**, e2021GB007042 (2022).
28. UN, "United Nations Scientific Committee on the Effects of Atomic Radiation. Sources and Effects of Ionizing Radiation – Volume 1: Sources. UNSCEAR 2000 Report to the General Assembly, with Scientific Annexes. ISBN: 92-1-142238-8.," (United Nations, New York, 2000).
29. H. K. Gibbs, A. Ruesch, "New IPCC Tier-1 Global Biomass Carbon Map for the Year 2000. CDIAC, ESS-DIVE repository. Dataset. doi:10.15485/1463800," (2008).
30. S. A. Spawn, C. C. Sullivan, T. J. Lark, H. K. Gibbs, Harmonized global maps of above and belowground biomass carbon density in the year 2010. *Scientific Data* **7**, 112 (2020).
31. K.-H. Erb *et al.*, Unexpectedly large impact of forest management and grazing on global vegetation biomass. *Nature* **553**, 73-76 (2018).
32. P. B. Reich *et al.*, Temperature drives global patterns in forest biomass distribution in leaves, stems, and roots. *Proceedings of the National Academy of Sciences* **111**, 13721-13726 (2014).
33. Z. Shi *et al.*, The age distribution of global soil carbon inferred from radiocarbon measurements. *Nature Geoscience* **13**, 555-559 (2020).
34. C. Beer *et al.*, Terrestrial gross carbon dioxide uptake: global distribution and covariation with climate. *Science* **329**, 834-838 (2010).
35. L. R. Welp *et al.*, Interannual variability in the oxygen isotopes of atmospheric CO2 driven by El Nino. *Nature* **477**, 579-582 (2011).
36. G. Badgley, L. D. L. Anderegg, J. A. Berry, C. B. Field, Terrestrial gross primary production: Using NIRV to scale from site to globe. *Global Change Biology* **25**, 3731-3740 (2019).
37. M.-C. Liang *et al.*, New constraints of terrestrial and oceanic global gross primary productions from the triple oxygen isotopic composition of atmospheric CO2 and O2. *Scientific Reports* **13**, 2162 (2023).
38. J. M. Mathias, A. T. Trugman, Climate change impacts plant carbon balance, increasing mean future carbon use efficiency but decreasing total forest extent at dry range edges. *Ecol Lett* **25**, 498-508 (2022).
39. N. Wei *et al.*, Evolution of Uncertainty in Terrestrial Carbon Storage in Earth System Models from CMIP5 to CMIP6. *Journal of Climate* **35**, 5483-5499 (2022).
40. A. Wolf *et al.*, Forest biomass allometry in global land surface models. *Global Biogeochemical Cycles* **25**, (2011).
41. R. A. Fisher *et al.*, Vegetation demographics in Earth System Models: A review of progress and priorities. *Global Change Biology* **24**, 35-54 (2018).
42. J. A. Lutz *et al.*, Global importance of large-diameter trees. *Global Ecology and Biogeography* **27**, 849-864 (2018).
43. T. Naegler, I. Levin, Biosphere-atmosphere gross carbon exchange flux and the $\delta^{13}CO_2$ and $\Delta^{14}CO_2$ disequilibria constrained by the biospheric excess radiocarbon inventory. *J Geophys Res* **114**, D17303 (2009).
44. Y. He *et al.*, Radiocarbon constraints imply reduced carbon uptake by soils during the 21st century. *Science* **353**, 1419-1424 (2016).
45. Y. Luo *et al.*, Matrix Approach to Land Carbon Cycle Modeling. *Journal of Advances in Modeling Earth Systems* **14**, e2022MS003008 (2022).

46. H. Metzler *et al.*, Mathematical Reconstruction of Land Carbon Models From Their Numerical Output: Computing Soil Radiocarbon From C Dynamics. *Journal of Advances in Modeling Earth Systems* **12**, e2019MS001776 (2020).
47. S. Khatiwala, Fast Spin-Up of Geochemical Tracers in Ocean Circulation and Climate Models. *Journal of Advances in Modeling Earth Systems* **15**, e2022MS003447 (2023).
48. C. D. Jones *et al.*, C4MIP – The Coupled Climate–Carbon Cycle Model Intercomparison Project: experimental protocol for CMIP6. *Geosci Model Dev* **9**, 2853-2880 (2016).
49. CMIP5 and CMIP6 data available at: https://esgf-node.llnl.gov/projects/esgf-llnl/

Acknowledgments: We dedicate this paper to the memory of Ingeborg Levin, a pioneering, dedicated and beloved scientist whose ambitions and efforts to measure and use ^{14}C to understand the carbon cycle laid the foundation for this study. We acknowledge the CESM2 Large Ensemble Community Project and supercomputing resources provided by the IBS Center for Climate Physics in South Korea. We acknowledge the World Climate Research Programme, which, through its Working Group on Coupled Modelling, coordinated and promoted CMIP6 and CMIP5. We thank the climate modeling groups for producing and making available their model output, the Earth System Grid Federation (ESGF) for archiving the data and providing access, and the multiple funding agencies who support CMIP6, CMIP5 and ESGF.

Funding:

Leverhulme Trust, Philip Leverhulme Prize PLP-2018-038

Royal Society Wolfson Fellowship RSWF\FT\191013

Eric and Wendy Schmidt by recommendation of the Schmidt Futures program for LEMONTREE (Land Ecosystem Models based On New Theory, obseRvations and ExperimEnts)

Director, Office of Science, Office of Biological and Environmental Research of the US Department of Energy under contract DE-AC02-05CH11231 through the Regional and Global Model Analysis (RUBISCO SFA) and Environmental Systems Science (NGEE-Tropics) Programs

Author contributions:

Conceptualization: HDG

Methodology: HDG, HW, CK, WW

Investigation: HDG, HW, HKG, SK, CK, JL, IL, SS, WW

Visualization: HDG, JL

Writing – original draft: HDG

Writing – review & editing: HDG, HW, HKG, SK, CK, JL, IL, SS, WW

Competing interests: Authors declare that they have no competing interests.

Data and materials availability: CMIP5 and CMIP6 model output data are available at (*49*). CLM5.0 data are available at (*23*) and CESM2-LENS data are available at (*26*). Other data are available from the listed references (*11*, *13-18*, *28-31*). All data plotted in figures in this manuscript are tabulated in Data S1 as an Excel spreadsheet.

Supplementary Materials

Materials and Methods

Figs. S1 to S6

Tables S1 to S2

Data S1

Fig. 1. Budget of excess ^{14}C from nuclear bomb testing. (a) Accumulation of ^{14}C in the stratosphere (*11*), troposphere (*13, 14*) and ocean since 1950 based on observations, and simulated accumulation of ^{14}C in ocean models (*15-17*) selected to match observations (*19, 20*) in the 1970s and 1990s. Inset shows annual nuclear bomb strength in units of Mt TNT equivalent (*28*). The period 1963-67 with no significant bombs is highlighted in green. (b) ^{14}C accumulation in the stratosphere, troposphere and ocean since 1963, focusing on the period 1963-67 with no significant nuclear detonations (green area in a.). The black solid line shows an exponential fit to the stratospheric data and the dashed lines show the 1-σ uncertainty in the χ^2 fit. (c) Our new observation-based estimate of ^{14}C accumulation in the terrestrial biosphere in 1967 relative to 1963 (black circle), based on the budgeting approach, and simulations of the CLM5.0 model driven with observed climate data (CLM5.0-unc) or as part of the CESM2 model in the Large Ensemble (CESM2-LENS). The black area shows the range of ^{14}C accumulation in the terrestrial biosphere across 9 ensemble members. ^{14}C accumulation in vegetation, soils and litter (including coarse woody debris) are shown for CESM2-LENS ensemble member 1001.001.

Figure 2. Model-data comparison for vegetation in the emulator models and in CESM2. (a) Simulated accumulation of ^{14}C in vegetation since 1963 compared with the observation-based estimate of ^{14}C accumulation in vegetation over 1963-67. (b) Accumulation of ^{14}C in vegetation over 1963-67 vs NPP in 1965 in each emulator model and CESM2, including a regression line for emulator models excluding MRI models. Gray area shows the uncertainty range in the observation-based estimate of ^{14}C accumulation. (c) Accumulation of ^{14}C in vegetation over 1963-67 vs carbon stock in vegetation in 2010 (2005 for MRI1 and IPSL5) in each emulator model and CESM2, including observation-based estimates of vegetation carbon stock (*29-31*) where the gray area reflects the uncertainty from Erb et al. (*31*) and uncertainty in ^{14}C accumulation. (d) and (e) show histograms of NPP in 1965 and carbon stock in vegetation in 2010 in CMIP6 models, including additional models that could not be included in the vegetation emulator simulations because the available CMIP6 output for these models lacked the necessary variables to run the emulator model (Table S2). The explicit simulation of ^{14}C in vegetation in CESM2-LENS member 1001.001 (CESM2-LENS1) is shown in (a-c) for comparison with the CESM2 vegetation emulator model.

Figure 3. Sensitivity of ^{14}C accumulation to NPP and total carbon. Accumulation of ^{14}C over 1963-67 in non-woody (a) and woody (b) vegetation biomass plotted in color with NPP and total carbon stock in 1965 on x and y axes. Contours reflect relationships across 16 simulations of the CESM2 emulator where NPP and total carbon stock were scaled across the range shown here. Symbols show ^{14}C accumulation in the emulator models using the same color bar.

Fig. 4. Spatial distribution of ^{14}C accumulation simulated in vegetation in the emulator models and in CESM2. Accumulation of ^{14}C over 1963-67 per degree latitude in total (a), non-woody (b) and woody (c) vegetation biomass integrated over all longitudes. The explicit

simulation of ^{14}C in CESM2-LENS1 is shown in (a) for comparison with the CESM2 emulator model.

"Figure #1"

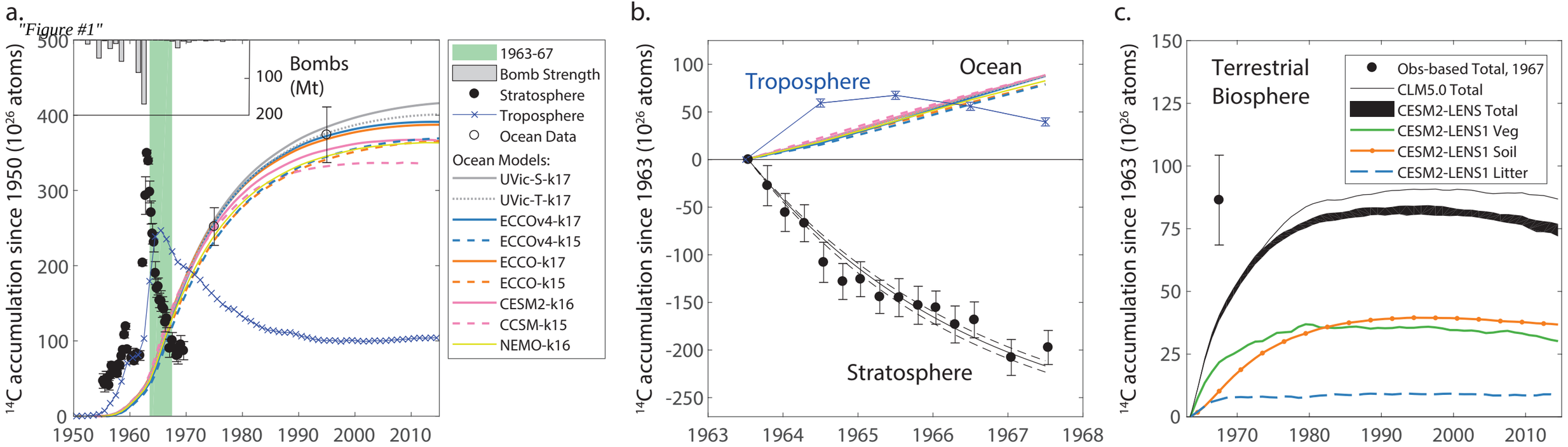
a.
b.
c.
^{14}C accumulation since 1950 (10^{26} atoms)
^{14}C accumulation since 1963 (10^{26} atoms)
Bombs (Mt)
100
200
1963-67
Bomb Strength
Stratosphere
Troposphere
Ocean Data
Ocean Models:
UVic-S-k17
UVic-T-k17
ECCOv4-k17
ECCOv4-k15
ECCO-k17
ECCO-k15
CESM2-k16
CCSM-k15
NEMO-k16
Troposphere
Ocean
Stratosphere
Terrestrial Biosphere
Obs-based Total, 1967
CLM5.0 Total
CESM2-LENS Total
CESM2-LENS1 Veg
CESM2-LENS1 Soil
CESM2-LENS1 Litter

"Figure #2"

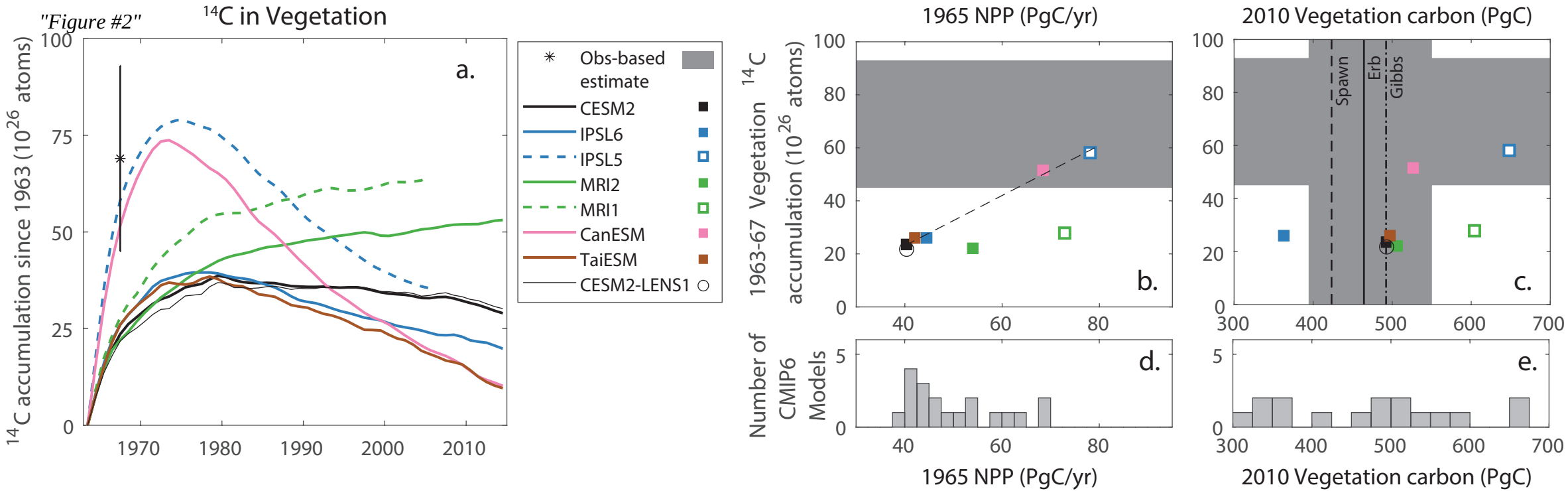
14C in Vegetation
a.
14C accumulation since 1963 (10^26 atoms)
100
75
50
25
0
1970
1980
1990
2000
2010
Obs-based estimate
CESM2
IPSL6
IPSL5
MRI2
MRI1
CanESM
TaiESM
CESM2-LENS1
1965 NPP (PgC/yr)
1963-67 Vegetation 14C accumulation (10^26 atoms)
b.
Number of CMIP6 Models
d.
1965 NPP (PgC/yr)
2010 Vegetation carbon (PgC)
Spawn
Erb
Gibbs
c.
e.
2010 Vegetation carbon (PgC)

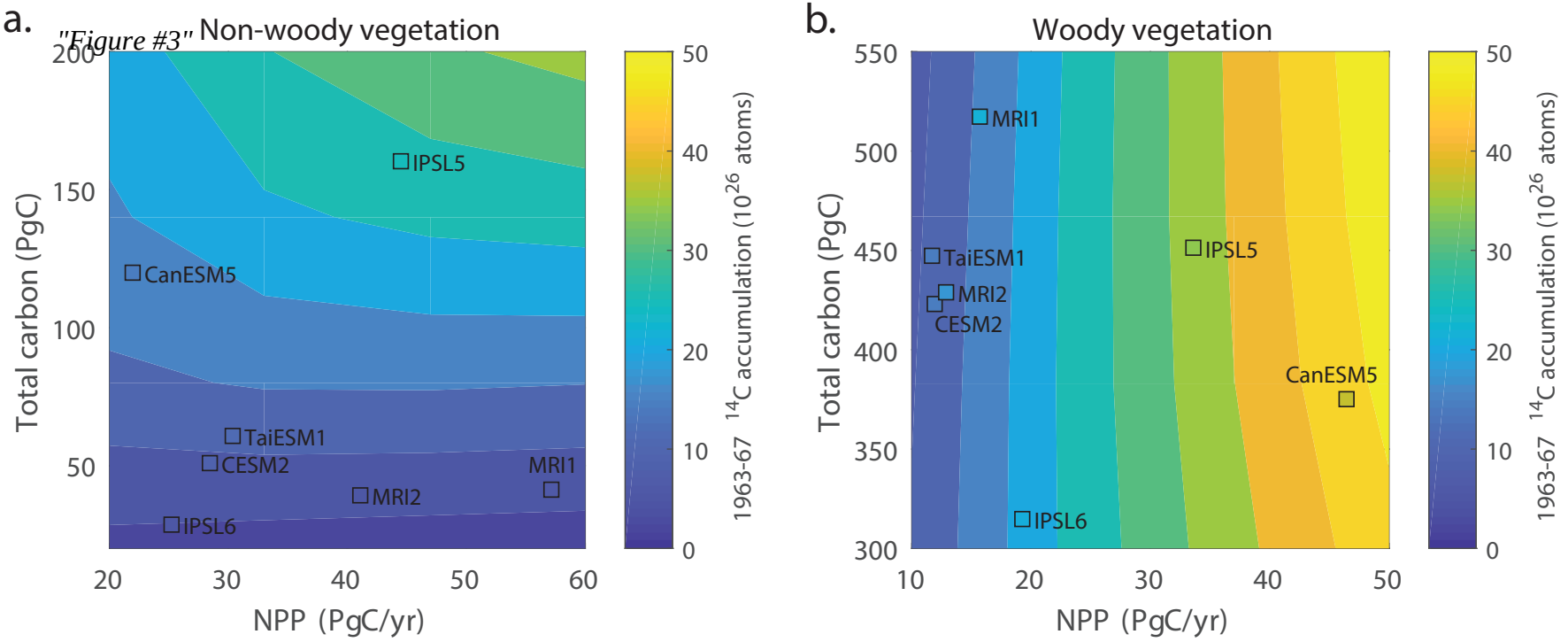
a.
"Figure #3"
Non-woody vegetation
Total carbon (PgC)
NPP (PgC/yr)
1963-67 14C accumulation (10^26 atoms)
IPSL5
CanESM5
TaiESM1
CESM2
MRI2
MRI1
IPSL6
b.
Woody vegetation
Total carbon (PgC)
NPP (PgC/yr)
1963-67 14C accumulation (10^26 atoms)
MRI1
TaiESM1
MRI2
CESM2
IPSL5
CanESM5
IPSL6

"Figure #4"

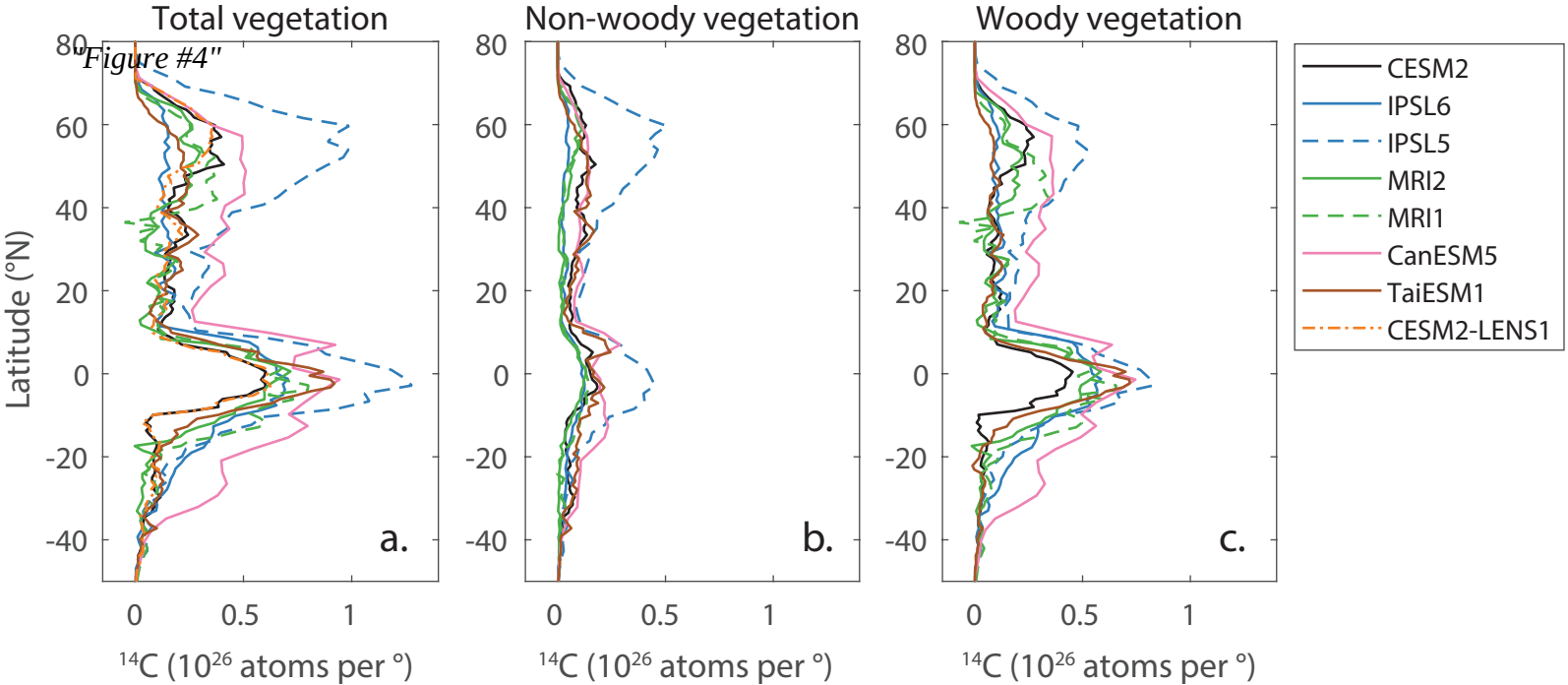
Total vegetation
Non-woody vegetation
Woody vegetation
Latitude (°N)
80
60
40
20
0
-20
-40
0
0.5
1
a.
b.
c.
^{14}C (10^{26} atoms per °)
CESM2
IPSL6
IPSL5
MRI2
MRI1
CanESM5
TaiESM1
CESM2-LENS1

Science
AAAS

Supplementary Materials for

Bomb radiocarbon evidence for strong global carbon uptake and turnover in terrestrial vegetation

Heather D. Graven, Hamish Warren, Holly K. Gibbs, Samar Khatiwala, Charles Koven, Joanna Lester, Ingeborg Levin, Seth A. Spawn-Lee, and Will Wieder

Corresponding author: h.graven@imperial.ac.uk

The PDF file includes:

Materials and Methods
Figs. S1 to S6
Tables S1 to S2

Other Supplementary Materials for this manuscript include the following:

Data S1

Materials and Methods

Uncertainty estimation for ^{14}C accumulation in the terrestrial biosphere and in vegetation

The ^{14}C accumulation in the terrestrial biosphere over 1963-67 and its uncertainty ($86 \pm 18 \times 10^{26}$ atoms, 95% confidence, Figure 1c) is calculated as the residual between the ^{14}C changes in the stratosphere, troposphere and ocean in 1000 Monte Carlo simulations. In each simulation, one ocean model was selected randomly from the group in Figure 1b. Normally distributed random errors were applied to the stratospheric and tropospheric ^{14}C accumulation, based on an exponential χ^2 fit to the stratospheric data and an uncertainty of 4×10^{26} atoms (1-σ) in tropospheric data (*11*). A possible positive bias of up to 5% could be present in the stratospheric data (*9, 10*), and this uncertainty was modelled with a uniform distribution between 0 and 5% in the Monte Carlo simulations. The mean and 95% confidence range of the ^{14}C accumulation in the terrestrial biosphere over 1963-67 across the Monte Carlo simulations is $86 \pm 18 \times 10^{26}$ atoms. The troposphere is considered to be 80% of the atmosphere.

The ^{14}C accumulation in vegetation over 1963-67 ($69 \pm 24 \times 10^{26}$, 95% confidence, Figure 2a) was calculated by subtracting the simulated ^{14}C accumulation in litter, coarse woody debris and soils in the CESM2 model from the above observation-based result for ^{14}C accumulation in the terrestrial biosphere. An uncertainty of 50% (1-σ) was estimated for the ^{14}C accumulation in litter, coarse woody debris and soils because this allows for a range of nearly zero to 200% at 95% confidence. The resulting fraction of terrestrial ^{14}C accumulation in vegetation as opposed to litter, coarse woody debris and soils is 43-100 %. We believe this estimate is conservative as it is unlikely that all of the ^{14}C in the terrestrial biosphere was in vegetation, but also unlikely that much less than half was in vegetation. The peak in tropospheric $\Delta^{14}C$ occurred only in 1964-65, during the period we consider, and the ^{14}C must first enter vegetation before passing into litter and soil pools. In addition, (*33*) demonstrated that CESM2 (CLM5) overestimates the $^{14}C/C$ ratio of both surface and sub-surface soils, showing that the proportion of fresh carbon in soil is already too high.

Analysis of explicit ^{14}C simulations from CESM2 and CLM5

Radiocarbon is simulated explicitly in CLM5, the land component of the CESM2 model (*22, 24*), and output from historical runs of the CESM2-LENS following CMIP6 protocol are available from (*26*). CLM5-unc used GSWP3 climate data forcing (http://hydro.iis.u-tokyo.ac.jp/GSWP3/) and output is available from (*23*).

To calculate the ^{14}C accumulation in CESM2 and CLM5 (Figure 1) we used the output variables C14_TOTECOSYSC, C14_TOTVEGC, and C14_TOTSOMC that provide gridded values of ^{14}C in g ^{14}C m^{-2} for total ecosystem carbon, vegetation carbon and soil carbon, respectively. ^{14}C in litter and coarse woody debris is given by the difference of C14_TOTECOSYSC and TOTVEGC and TOTSOMC. We note the ^{14}C output from CESM2 and CLM5 is reported in units of g ^{14}C, however, the atomic weight used in the model is 12 g/mol rather than 14 g/mol. Therefore, in the conversion from g to atoms ^{14}C we used 12 g/mol. In addition, the value of the standard $^{14}C/C$ ratio used in CESM2 and CLM5 is 1.0×10^{-12} rather than the accepted value of 1.176×10^{-12}. Therefore, we multiplied the ^{14}C output by 1.176. To calculate the global ^{14}C accumulation we summed over all grid cells, after multiplying by the grid cell area (given by

variable area) and land fraction (given by variable landfrac), and took the difference from the year 1963.

Description of model emulator for vegetation ^{14}C

While it was not possible to construct complete ecosystem model emulators for other CMIP models using the output variables available, we did construct model emulators for vegetation. The vegetation emulator model considers two parallel boxes representing woody and non-woody vegetation and is run for each grid cell in the model.

The CMIP variables npp, nppWood, cVeg and cWood were used to calculate NPP to non-woody vegetation and carbon in non-woody vegetation (nppNonWood=npp-nppWood and cNonWood=cVeg-cWood). Then ordinary differential equations for ^{14}C in wood ($^{14}C_w$) and non-wood ($^{14}C_{nw}$) vegetation are:

1) $$\frac{d^{14}C_w}{dt} = R_A\, nppWood - \frac{^{14}C_w}{cWood}\left(nppWood - \frac{d\,cWood}{dt}\right) - \frac{^{14}C_w}{8267}$$

2) $$\frac{d^{14}C_{nw}}{dt} = R_A\, nppNonWood - \frac{^{14}C_{nw}}{cNonWood}\left(nppNonWood - \frac{d\,cNonWood}{dt}\right) - \frac{^{14}C_{nw}}{8267}$$

where R_A is the $^{14}C/C$ ratio in atmospheric CO_2 in three zonal bands (*13*). R_A was calculated as $\Delta^{14}C/1000‰+1$ without accounting for $\delta^{13}C$. The model preserves the carbon accumulation in the ESM, which was checked by constructing a similar emulator model for carbon only.

The emulator model was coded in Matlab and run for each native grid cell in each model using the ode15s solver. The simulations were spun up for 1849 years using annual mean npp, nppWood, cVeg and cWood values for 1850. Simulations were then run over 1850 to 2005 or 2014, depending on the end year of the model output. For CESM2, output from LENS member 1001.001 was used. The models in addition to CESM2 that were run in the vegetation emulator model are listed in Table S1.

For the MRI models, there was an error in the nppWood output files. nppWood was corrected by the following equation, following the advice of M. Hosaka.

3) $$nppWood = npp\,\frac{nppWood}{nppWood + nppLeaf + nppRoot}$$

The following provides an example code snippet for the Matlab code used to run the emulator model on an individual grid cell, where din_gc gives the annual mean NPP, carbon stock and flux out for woody and non-woody pools in that grid cell from the ESM. The initial conditions are given by y0 (zeros) and the period of simulation is given in years by tspan (year 1.5 to either 2005.5 or 2014.5).

```
[~,y] = ode15s (@(t,y) em14C_veg(t,y,din_gc,atmosIn,aTime,allvars) ,tspan,y0);

function a = em14C_veg(t,y,dm,atmosData,atmosTime,vars)
% 2 box vegetation emulator model
% keeping a factor of Rstd=1.176x10^-12
% outgoing flux fx is defined previously as the difference between input and accumulation

a=zeros(2,1); % Initialize output variables
```

```
% Interpolate data
if t<1850.5
   D14C = atmosData(1);
   for v = 1:length(vars)
      m.(vars{v}) = dm(v,1);
   end
else
   D14C = interp1(atmosTime,atmosData,t);
   for v=1:length(vars)
      m.(vars{v})=interp1(1850.5:1849.5+length(dm(v,:)),dm(v,:),t);
   end
end

% define R atmosphere
RA=(D14C/1000+1);
% differential equations:
a(1) = RA * m.nppWood - (y(1) / m.cWood) * m.fxWood - y(1)/8267;
a(2) = RA * m.nppNotwood - (y(2) / m.cNotwood) * m.fxNotwood - y(2)/8267;
```

Sensitivity experiments for vegetation in CESM2

Sixteen sensitivity experiments were run in the CESM2 vegetation emulator model to understand the relationship between the ^{14}C inventory, NPP and total carbon in woody and non-woody vegetation. NPP and total carbon in each grid cell were scaled by a fixed amount in all years to produce global values in 1965 of 10, 23, 37 and 50 PgC NPP and 300, 383, 467 and 550 PgC of total carbon in wood, and 20, 33, 47, 60 PgC/yr in NPP and 20, 80, 140 and 200 PgC of total carbon in non-woody vegetation. All combinations of these values were simulated, in sixteen different simulations. The range of values chosen was guided by the range in the CMIP models (Figure 3, Table S1).

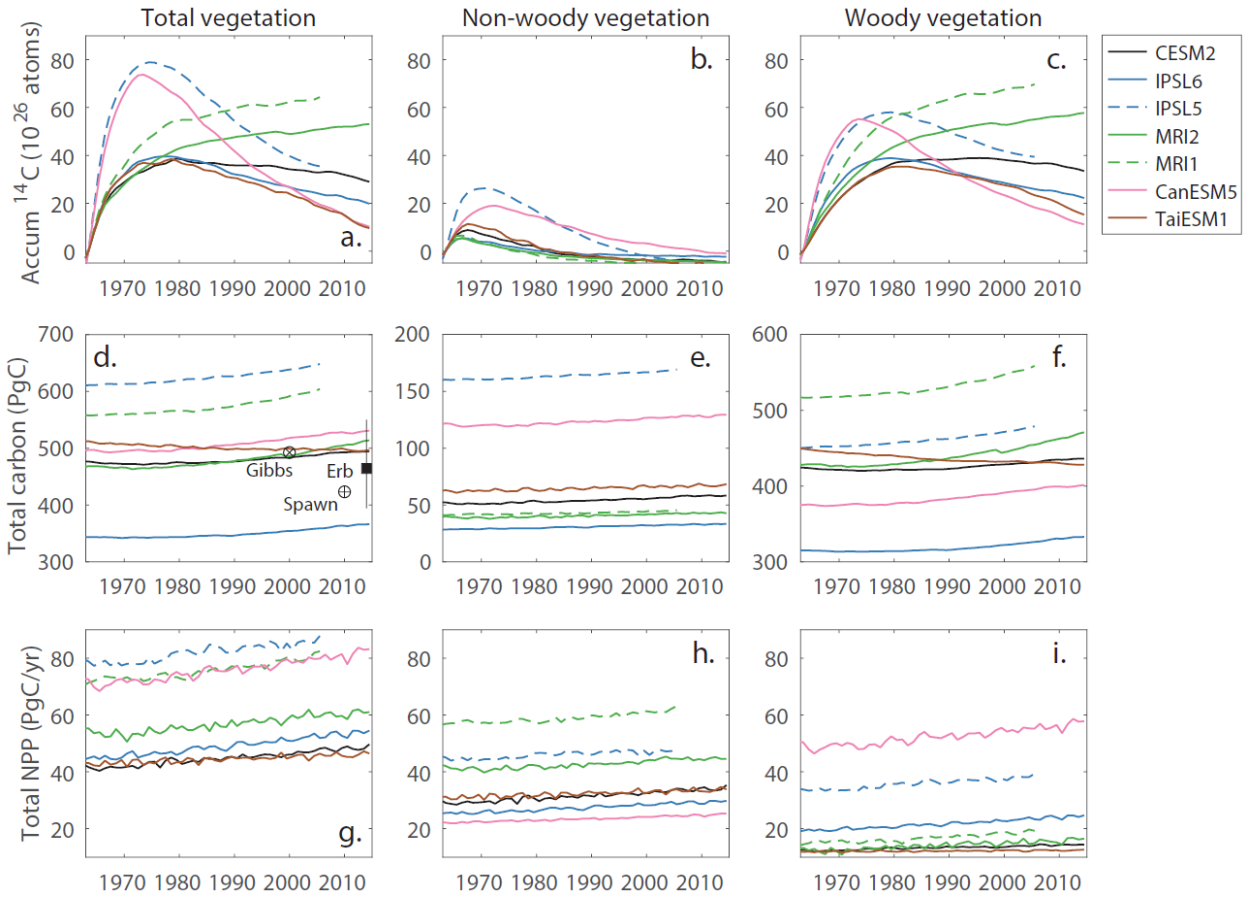

Fig. S1. Accumulation of ^{14}C since 1963 in total (a), non-woody (b) and woody (c) vegetation in CESM2 and the CMIP vegetation emulator models. Carbon stock in total (d), non-woody (e) and woody (f) vegetation biomass, including observation-based estimates of total vegetation carbon from Erb et al. (*31*), Gibbs and Ruesch (*29*), and Spawn et al. (*30*) in (d). These observation-based vegetation carbon products omit leaf carbon in forests so we estimated global total leaf carbon in forests to be 14.3 PgC (based on Table S5 in reference (*32*)) and added this to the observation-based vegetation carbon stocks. NPP in total (g), non-woody (h) and woody (i) vegetation.

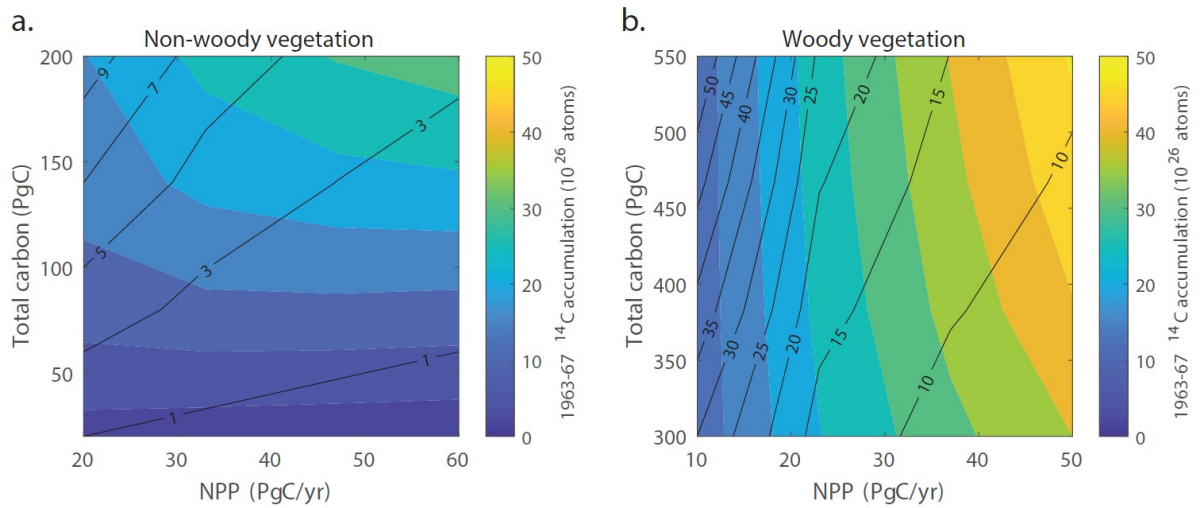

Fig. S2. Accumulation of ^{14}C in non-woody and woody vegetation over 1963-67 in the sensitivity experiments with the CESM2 emulator model. Colors show ^{14}C accumulation over 1963-67 and isolines show turnover time (total carbon/NPP, inverse of turnover rate) in 1965.

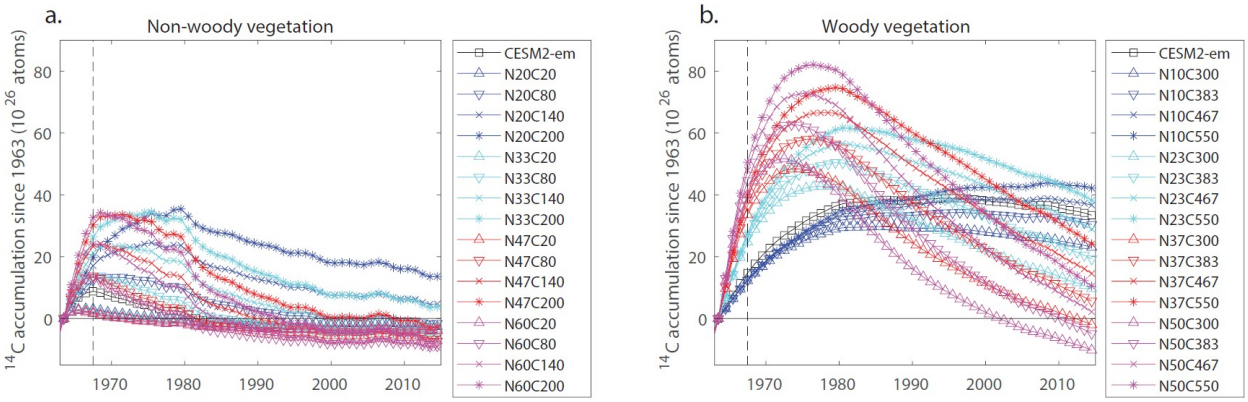

Fig. S3. Accumulation of ^{14}C in non-woody vegetation (a) and woody vegetation (b) in the sensitivity experiments with the emulator model for CESM2. Different colors reflect different NPP and different symbols reflect different total carbon stock. 1967 is indicated with a vertical dashed line.

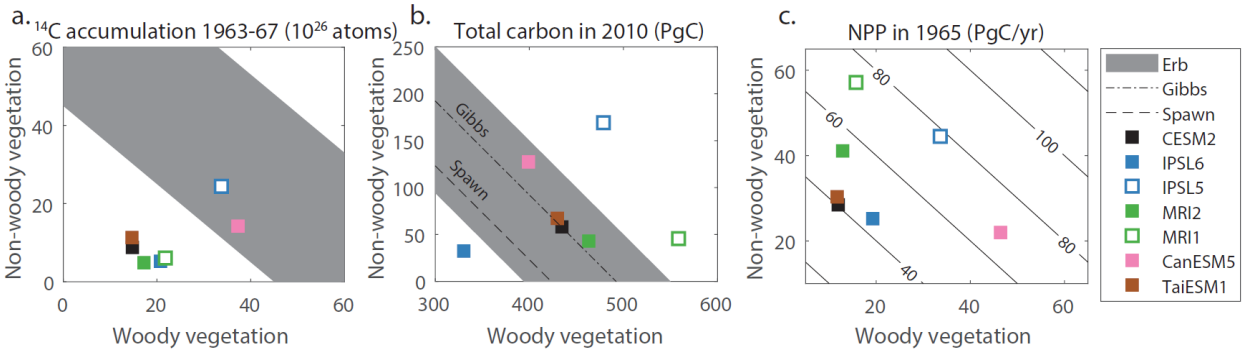

Fig. S4. Non-woody vegetation vs woody vegetation simulations with observation-based estimates for bomb ^{14}C inventory in 1965 (a), total carbon stock in 2010 (b, 2005 for MRI1 and IPSL5) and NPP in 1965 (c). Observation-based estimates for vegetation bomb ^{14}C inventory from this work are included in (a). Observation-based estimates for total vegetation carbon stocks are included as lines in (b) from Erb et al. (*31*) (gray area), Gibbs and Ruesch (*29*) (dash-dotted line), and Spawn et al. (*30*) (dashed line) without accounting for the different likelihoods of particular combinations of woody and non-woody carbon stocks. These observation-based vegetation carbon products omit leaf carbon in forests so we estimated global total leaf carbon in forests to be 14.3 PgC (based on Table S5 in reference (*32*)) and added this to the observation-based vegetation carbon stocks. Lines in (c) show isolines of total NPP for reference.

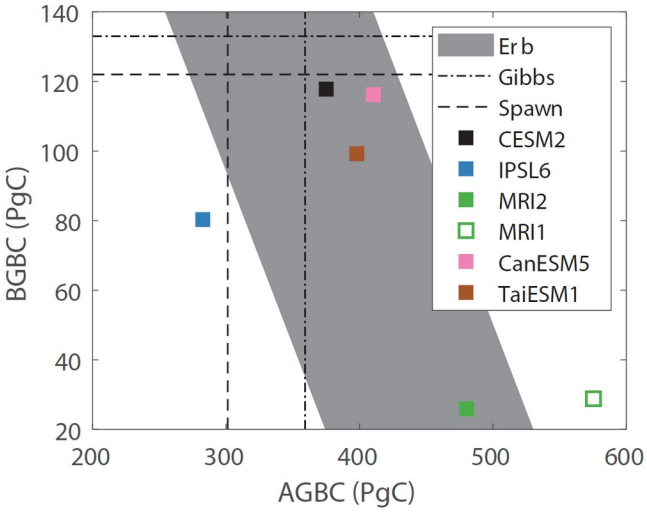

Fig. S5. Below ground biomass carbon (BGBC) vs above ground biomass carbon (AGBC) in 2010 (2005 for MRI1) in the CMIP models used for the emulator models and in the observation-based estimates from Gibbs and Ruesch (*29*), and Spawn et al. (*30*). Observation-based estimates of total vegetation carbon stocks from Erb et al. (*31*) are included without accounting for the different likelihoods of particular combinations of AGBC and BGBC carbon stocks. These observation-based vegetation carbon products omit leaf carbon in forests so we estimated global total leaf carbon in forests to be 14.3 PgC (based on Table S5 in reference (*32*)) and added this to the observation-based AGBC.

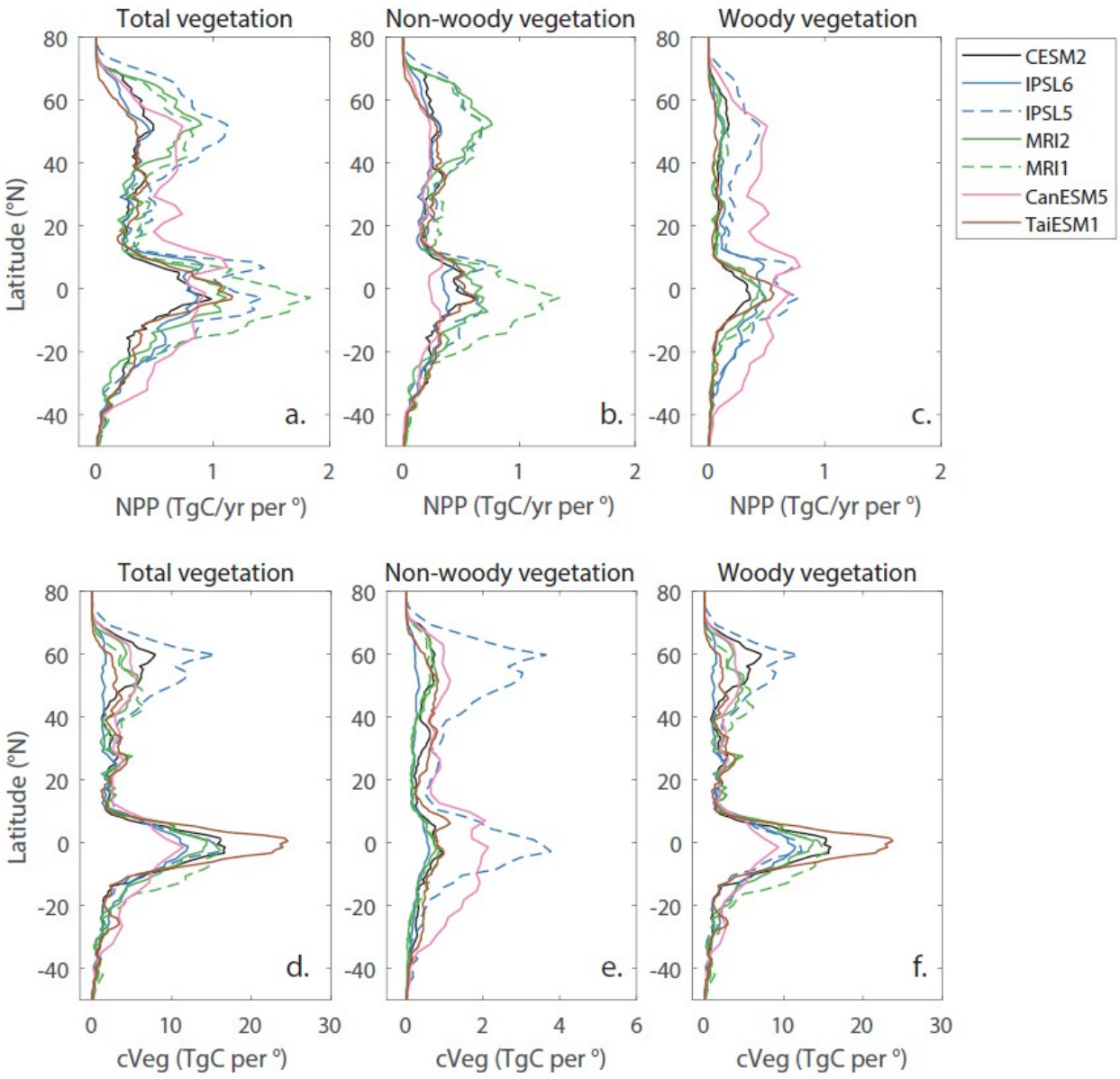

Fig. S6. NPP and total stock of carbon for 1965 per degree latitude in total (a and d), non-woody (b and e), and woody (c and f) vegetation biomass integrated over all longitudes.

Table S1. Details of CESM2 and CMIP5 and CMIP6 models used in emulator simulations of ^{14}C in vegetation. The last two models are from CMIP5 and the rest are from CMIP6. Outputs are from the 'historical' simulation and variables are shown for the year 1965. Non-woody and woody NPP fractions are shown in parentheses. Tau is the turnover time given by the carbon stock divided by the NPP.

Model	Variant ID	Total NPP (PgC/yr)	Non-woody NPP (PgC/yr)	Woody NPP (PgC/yr)	Total biomass (PgC)	Non-woody Biomass (PgC)	Woody Biomass (PgC)	Non-woody tau (yr)	Woody tau (yr)
CESM2-LENS	1001.001	40.3	28.4 (0.70)	11.9 (0.30)	474	51	423	1.8	36
IPSL-CM6A-LR	r1i1p1f1	44.5	25.2 (0.57)	19.3 (0.43)	343	28	315	1.1	16
MRI-ESM2-0	r1i2p1f1	54.0	41.1 (0.76)	12.9 (0.24)	468	39	429	1.0	33
CanESM5	r1i1p1f1	68.4	21.9 (0.32)	46.4 (0.68)	495	120	375	5.5	8
TaiESM1	r1i1p1f1	42.1	30.4 (0.72)	11.7 (0.28)	508	61	447	2.0	38
IPSL-CM5A-LR	r1i1p1	78.1	44.5 (0.57)	33.6 (0.43)	612	160	451	3.6	13
MRI-ESM1	r1i1p1	72.9	57.2 (0.78)	15.7 (0.22)	559	41	517	0.7	33

Table S2. NPP in 1965 and vegetation carbon in 2010 in CMIP6 models used in the histograms in Figure 2, in addition to the CMIP6 models listed in Table S1 above.

Model	Variant ID	NPP in 1965 (PgC/yr)	Vegetation carbon in 2010 (PgC)
ACCESS-ESM1-5	r1i1p1f1	43.8	670
AWI-ESM-1-1-LR	r1i1p1f1	47.5	255
BCC-ESM1	r2i1p1f1	53.7	475
CMCC-CM2-SR5	r1i1p1f1	40.8	413
CNRM-ESM2-1	r1i1p1f2	43.0	511
EC-Earth3-Veg	r1i1p1f1	49.5	343
GFDL-ESM4 *esm-hist	r1i1p1f1	51.7	344
GISS-E2-1-G	r1i1p3f1	42.5	Not available
INM-CM5-0	r1i1p1f1	68.9	654
MIROC-ES2L	r1i1p1f2	59.4	551
MPI-ESM1-2-LR	r1i1p1f1	64.9	375
NorESM2-LM	r1i1p1f1	39.4	476
SAM0-UNICON	r1i1p1f1	46.6	593
UKESM1-0-LL	r1i1p1f2	61.0	Not available

Data S1 (separate file). This Excel spreadsheet includes all of the data plotted in Figures 1-4 and Figures S1-S6. There is one sheet for each figure or figure panel. The source of the data is given with its reference or as "this work" for data generated in this study.